

# Intelligent modeling for estimating weld bead width and depth of penetration from infra-red thermal images of the weld pool

N. Chandrasekhar · M. Vasudevan ·  
A. K. Bhaduri · T. Jayakumar

Received: 16 October 2012 / Accepted: 18 March 2013 / Published online: 13 April 2013  
© Springer Science+Business Media New York 2013

**Abstract** In order to develop remote welding process methodologies, it is first important to develop computational methodologies employing soft computing techniques for predicting weld bead width and depth of penetration using a real time vision sensor during welding. Welding being a thermal processing method, sensing using infra-red (IR) camera is most extensively employed for monitoring and control of welding process. In the present work, attempt has been made to develop predictive methodologies using hybrid soft computing techniques for accurately estimating the weld bead width and depth of penetration from the IR thermal image of the weld pool. IR thermal images have been recorded in real time during A-TIG welding of 6 mm thick type 316 LN stainless steel weld joints with varying current values to produce different depth of penetration. From the acquired IR images, hot spot was identified by image segmentation using the cellular automata image processing algorithm for the first time. The current and the four extracted features from the hot spot of the IR thermal images were used as inputs while the measured bead width and depth of penetration were chosen as the output of the respective adaptive neuro fuzzy inference system and artificial neural network based models. Independent models were developed for estimating weld bead width and depth of penetration respectively. There was good correlation between the measured and estimated values of bead width and depth of penetration using the developed models.

**Keywords** Welding · Infra-red thermal image · Cellular automata · Image processing · ANFIS · ANN · Weld bead width and depth of penetration

## Introduction

As most of the structural components of the operating nuclear reactors are fabricated by welding and life extension or modifications to its structural component require remote repair welding to ensure that nuclear plant can continue to run safely and efficiently without exposing personnel to the radiation environment. Hence, it is essential to develop remote repair welding process methodologies for carrying out remote repair welding of structural components. The welding processes most widely used for repair welding in nuclear power plants include tungsten inert gas (TIG) welding, metal active gas (MAG) welding and shielded metal arc welding (SMAW) processes. TIG welding process can be used remotely however it does not produce deep penetration welds. The process is slow and requires quite a number of welding passes to complete single welded joint. The TIG welding process is prone to variable weld penetration due to minor variations in the chemical composition of austenitic stainless steels and also requires a separate wire feeder system. The use of MAG welding process is limited to C-Mn steel components only. New processes which find application in remote repair welding include high power Nd:YAG laser and TIG welding with activated fluxes which all have potential for improved performance. Nd:YAG lasers offer delivery of the beam through fiber optics which allows flexible manipulation of welding head to deliver single pass deep penetration welds. TIG welding with activated fluxes also offers potential for producing deep penetration welds for remote repair welding applications.

Low carbon austenitic stainless steel types 304 and 316 alloyed with nitrogen, designated as 304L(N) and 316L(N) stainless steels are finding application as structural materials for nuclear reactors. Type 316LN stainless steel is chosen as high temperature structural material for the fabrication

N. Chandrasekhar · M. Vasudevan (✉) · A. K. Bhaduri · T. Jayakumar  
Metallurgy and Materials Group, Indra Gandhi Centre  
for Atomic Research, Kalpakkam 603102, India  
e-mail: dev@igcar.gov.in

of structural components of prototype fast breeder reactor (PFBR). Activated fluxes have been developed in-house for enhancing the penetration performance of TIG welding of austenitic stainless steel by 300% (Vasudevan 2007). A-TIG welding of austenitic stainless steels was found to mitigate the variable weld penetration during autogenous TIG welding. A-TIG welding process has been developed to achieve penetration up to 12 mm in single pass welding of type 316LN austenitic stainless steel (Vasudevan 2007). A-TIG welding process is one of the candidate process chosen for remote repair welding of nuclear structural components made of austenitic stainless steels.

In order to employ the above welding processes for remote repair welding applications, the use of sensing technology and adaptive control must also be considered. Vision sensing, in-process control and offline programming techniques are under development or currently employed for robotic remote repair welding. In manual welding process, the welder ensures the quality of the weld by monitoring and suitably manipulating the process parameters according to the changing environment based on his knowledge and experience. In the case of adaptive welding vision system, sensors play the role of welder. Several sensing techniques have been developed to monitor weld bead profile and depth of penetration which include acoustic sensors, ultrasonic sensors, optical sensors, vision sensors etc. (Sun and Kannatey-Asibu 1999). Acoustic sensor have been successfully developed to monitor laser welding of steels (Huang and Kovacevic 2009). It was possible to ascertain the status of the molten weld pool, the generated plasma, the vaporized metal, the key hole by monitoring the acoustic signals produced during the laser welding process. To improve the quality of acoustic signals in a noisy and hostile environment, it was necessary to apply noise reduction methods. After improving the quality of acoustic signals, it was feasible to monitor and control the laser welding process to achieve full penetration welds. Ultrasonic technique has been successfully used in directly measuring the weld pool geometry by employing non-contact laser based and electromagnetic acoustic transducers (Graham and Ume 1997). The authors found that the large temperature gradient within the heat affected zone can reflect ultrasonic waves thus limiting the accuracy of measuring the weld pool dimensions. Most of the optical sensing methods used have involved the use of laser/solid state camera and/or photo diode combination for seam tracking and weld pool geometry control (Wei Huang and Radovan Kovacevic 2011). Image processing was used to extract the weld pool size and joint configuration and neural network processed the information very fast. Therefore, cost effective weld inspection systems could be developed using optical sensors. Vision systems use the charge-coupled device (CCD)/infra-red (IR)/complementary metal oxide semiconductor (CMOS) cameras for monitoring weld pool size and

to control the welding parameters (Zhang 2008). The purpose is to capture real data from practical welding situations, which can then be used as input to computational simulation of welding manufacturing operations. Optical sensing techniques have been used for joint tracking and fill control (Kovacevic et al. 1995), weld pool width and profile control (Kovacevic and Zhang 1997). Most of these sensing techniques can supervise only one welding parameter efficiently. Therefore extensive control of several welding parameters using the available sensing techniques would result in the use of multiple sensors or commonly known as multisensory systems. Use of a single sensor to monitor several welding parameters minimizes these problems. Investigations have suggested that infrared thermography may be such a sensor. Welding, inherently being a thermal processing method, infrared sensing is a natural choice for weld process information (Farson et al. 1998). The basis for using infrared imaging lies in the fact that an ideal welding condition would produce surface temperature distribution that shows a regular and repeatable pattern. Any variation or perturbation should result in discernible change in the thermal profiles (Chen and Chin 1990; Nagarajan et al. 1992; Banerjee et al. 1995). IR sensing is not without its difficulties, such as the interference of arc radiation and welding electrode emissions, these interferences are mitigated by using either mechanical or optical means to filter the unwanted thermal emissions (Farson et al. 1998; Menaka et al. 2005; Vasudevan et al. 2010).

To ensure reliable weld quality during remote repair welding, weld bead width and depth penetration are the two key variables to be sensed and controlled. The estimation of weld bead shape parameters such as weld bead width and depth of penetration of the weld pool from the IR thermal video of a welding process is an intermediate step towards online control of the welding process. Many attempts have been made to develop computational methodologies using soft computing techniques for estimating the weld bead shape parameters as a function of welding process parameters (Ghanty et al. 2007; Gowtham et al. 2011; Nagesh and Datta 2010; Edwin Raja Dhas and Kumanan 2007; Hyunsung Park and Sehun Rhee 1999) as well as from the acquired IR thermal image (Nagesh and Datta 2010; Nagarajan et al. 1992). Major problem in the analysis of IR thermal images is to accurately identifying the hot spot by image segmentation and edge detection. Image segmentation algorithms such as fuzzy c-means (Ghanty et al. 2008) and k-means clustering algorithm (Subashini and Vasudevan 2012; Chokkalingham et al. 2012) have been used for identifying the hot spot in IR thermal images. However, Image segmentation by cellular automata (CA) is more popular and suitable for complex segments. CA image processing algorithm has been successfully employed for image segmentation and edge detection on medical images (Kazar and Slatnia 2011; Kumar and Sahoo 2010; Hamamci et al. 2010). CA method supports two-dimensional and multiple structure

P1	P2	P3
P8	P	P4
P7	P6	P5

**Fig. 1** Moore's neighborhood pattern

categories where the number of segments does not increase computational time or complexity. This ability makes it suitable for segmenting weld pool IR thermal images with complex cluster structures. Since CA is a simple to implement and an accurate method where each cell uniformly follows a set of or individual rules, this naturally makes it an efficient algorithm. However, no segmentation method is suitable for all kinds of images, and further there is no common algorithm accepted by all.

The CA approach was originally invented by Ulam and Von Neumann to evaluate the behavior of natural complex systems (Wolfram 1986). The CA is a computer algorithm that is basically discrete in space and time and operates on a lattice or grid of cells. It consists of a two-dimensional array of cells. Each of these cells can be in one of a finite number of possible states, updated in parallel according to a state transition function. In the past few years, the application of CA in image processing to extract the segmentation information has grown. The research shows that, it can be applied in various simulation contexts, for example, physical simulations, fire propagation, artificial life and medical image processing (Kazar and Slatnia 2011; Kumar and Sahoo 2010). Therefore, it appears as a natural tool for image processing due to its local nature and simple Moore's neighborhood implementation. The Moore's neighborhood pattern is as shown in Fig. 1.

The present work aims at developing hybrid intelligent models combining image processing with soft computing techniques such as adaptive neuro fuzzy inference system (ANFIS) and artificial neural network (ANN) for estimating the weld bead width and the depth of penetration from the IR thermal image of the weld pool. First time, attempt is being made to apply CA image processing algorithm to identify hot spot in the IR thermal image of the weld pool. IR thermal image of the weld pool is acquired online during A-TIG welding of 6 mm thick type 316LN stainless steel plate. An IR camera is made to move along with the torch during welding and capture the weld pool image in real time. From the recorded thermal image video, hot spot is identi-



**Fig. 2** GTAW setup with IR camera

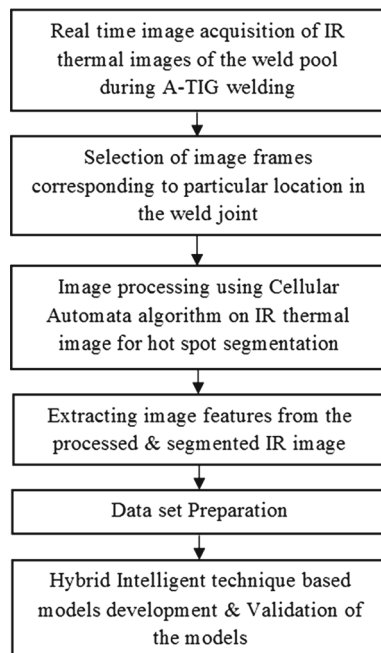
fied using CA image processing algorithm for the selected frames. Four image features are extracted and are used along with current values as input to the ANFIS and ANN models while the measured weld bead width and depth of penetration are used as output of the respective models. The predictive performance of the ANFIS and ANN models is compared in terms of the RMS errors.

## Experimental

The A-TIG welding was carried out on 6 mm thick 316LN austenitic stainless steel plates of dimension 300 mm long  $\times$  250 mm width to make square butt joint at various current values to achieve different depth of penetration values. The experimental setup for TIG welding is attached with an IR camera to facilitate real time monitoring of the weld pool during welding as shown in Fig. 2. The surface temperature distribution of the plate being welded is measured by the IR camera. The arc radiation and the radiation from hot tungsten electrode during TIG welding has been reported to occur in the spectral range of 0.34–1.8  $\mu\text{m}$  (Huang et al. 2007). In the present study, the IR thermography system measures temperature distribution by sampling portions of the emitted energy within a wavelength of range of 4.99–5.1  $\mu\text{m}$  using band pass filter, thereby suppressing the interference from the arc light and hot tungsten electrode on the image quality. The camera is capable of measuring temperature within the range of 473–1973 K, with an accuracy of  $\pm 1\%$  over the entire range. After welding, the weld joints were cut, samples were prepared and polished sequentially by automatic polishing machine to measure the actual weld bead width (BW) and depth of penetration (DOP) using a microscope. Welding process parameters used for making weld joints is given in Table 1. Thirty data points were generated from five different weld joints with different depth of penetration values. The samples were cut at specified locations of 60, 100, 140, 180, 220 and 260 mm respectively from the beginning of each of the weld joint.

**Table 1** GTAW welding parameters used for experiment

Process parameters	Range
Current	150–170 A
Welding speed (mm/min)	120 mm/s (constant)
Electrode	Tungsten electrode with 2 %
Electrode diameter	3.2 mm
Arc gap	1.5 mm (constant)
Shielding gas	Argon
Gas flow rate	10l/min
Electrode tip angle	45°

**Fig. 3** Flow chart for hybrid intelligent technique based model development

### Methodology of intelligent model development

The steps involved in the hybrid intelligent based model are given as flow chart in Fig. 3. The methodology involves image processing of the IR thermal images to identify the hot spot followed by feature extraction from the segmented images. CA image processing algorithm is proposed to be used to identify the hot spot region in the IR thermal image. After the image segmentation, the hot spot image is used for feature extraction. The extracted image features and the current used for welding will form the input variables of the ANFIS and ANN models. The measured weld bead width and depth of penetration will form the output variables of the respective models. During ANFIS model development, three membership functions namely triangular, Gaussian and bell shaped are used. The ANFIS model with a membership function producing minimum RMS test error is chosen for estimating

the weld bead width and depth of penetration. During ANN model development using back propagation neural network, L–M algorithm is proposed to be used. Independent models will be developed for estimating weld bead width and depth of penetration. Finally validation of the models will be carried out and the performance of the models in terms of the predicted RMS error will be assessed.

### Image acquisition and feature identification

To capture thermal images, JADE, CEDIP IR camera was used. It captures the image in a frame of size  $320 \times 240$  at a speed of 25 frames per second. It consists of built-in medium wave filter of the wave length range of  $4.99\text{--}5.1 \mu\text{m}$  to suppress beyond band width noises from infrared radiation during experiment and permits discrete intensities within the portion of the band width. The captured analog infrared magnitude is converted into discrete intensities by 14 bit analog to digital converter built in the camera. The captured intensity converted into temperature in the Altair software by factory calibrated block body setup files. These files are loaded for every experiment. The temporary stored current frames in the camera are communicated to PCI frame grabber in the higher-end personal computer by GPIB cable. The Altair software records the real time IR thermal images at a rate of 25 frames per second and saves into computer hard disk for further processing. The camera is mounted at an angle of  $45^\circ$  on the automatic TIG welding machine in the torch assembly. The mounted camera moves with the torch during welding to capture the weld pool image in real time. From the acquired IR thermal video, the video frame corresponding to the particular cut section is identified and called as the key frame at a particular time (which is shown in Fig. 6a). These key frames can be identified from the torch speed and the video frame rate. For example, for the welding experiment with torch speed of 2 mm/s and frame rate of 25 frames/s, the video frame corresponding to the cut section at 60 mm will be  $(60/2) \times 25 = 750\text{th}$  frame. Therefore, for each cut section, the corresponding key frame is identified. The extracted key frames were used further for image processing using CA to identify the hot spot.

### Image processing using cellular automation

The steps involved in the algorithm involve first capturing the weld pool IR image as a frame in real time by IR camera. Next the captured images were processed for filtering the noises in the captured image for further implementation of CA algorithm. The sources of noise in the weld pool image are due to background noises, unstable information and random disturbances. It does not reflect the true intensity value of pixel in magnitude of IR image. In order to achieve better quality image without losing valuable details, average filter



Fig. 4 CA mapping formats for selection of central cell

is used for removing such noises. In our algorithm to filter noises a two dimensional average filter was used by 'fspecial' Matlab command to enhance the smoothness of the segmented boundary region and thereby improve the quality of the IR thermal image of the selected key frame. During image processing the processed IR key frame is analyzed into pixels. With IR key frame images as gray scale images, each pixel indicates the magnitude of brightness to the image in a particular spot (0 indicates black, 255 indicate white). The main idea for using CA algorithm is to use the neighborhood relation of weld pool image matrix to make a better decision and thus to improve the accuracy of hot spot identification.

In the process of CA algorithm, a null value of an empty row and column were padded around the above filtered IR image matrix to facilitate propagation of CA mapping matrix. The CA mapping matrix were created equivalent to dimensions of the Moore's neighborhood option and then it was allowed to propagate around the entire image. The CA mapping matrix approach is equivalent to Moore's neighborhood pattern, contains nine neighborhood cells (P1–P8) and central cell is (P) as shown in Fig. 1. Each cell contains the magnitude intensity of IR image. Selection or de-selection of the central cell is based on its neighborhood states and transition rule. The transition rule is based on comparison criteria of a sum and difference between A and B set of variables to a threshold value as shown in Fig. 4. The threshold value was calibrated precisely to get accurate results of the segmented image. If the central cell is meeting the above criteria then it is selected as a hot spot region otherwise it is deselected. Figure 4 shows the various formats considered for selection of central cell. Applying these steps on overall image, the central cell converges and helps in identifying the hot spot segment region on the weld pool image and the algorithm stops. The proposed flow chart of CA algorithm is as shown in Fig. 5. The Fig. 6a shows a sample IR key frame and the typical extracted hot spot segment for the gray scale IR thermal image using CA is shown in Fig. 6b. The proposed CA algorithm programming code was developed in Matlab environment, and analytical results were processed in the Origin software.

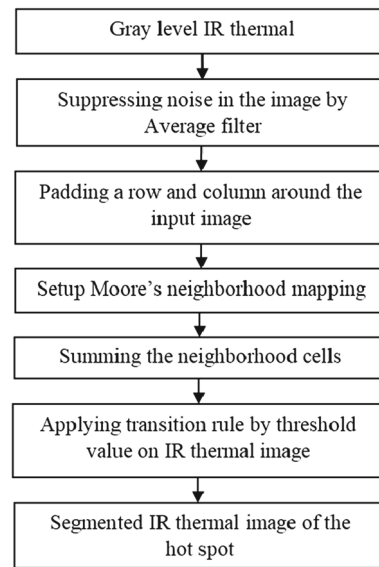
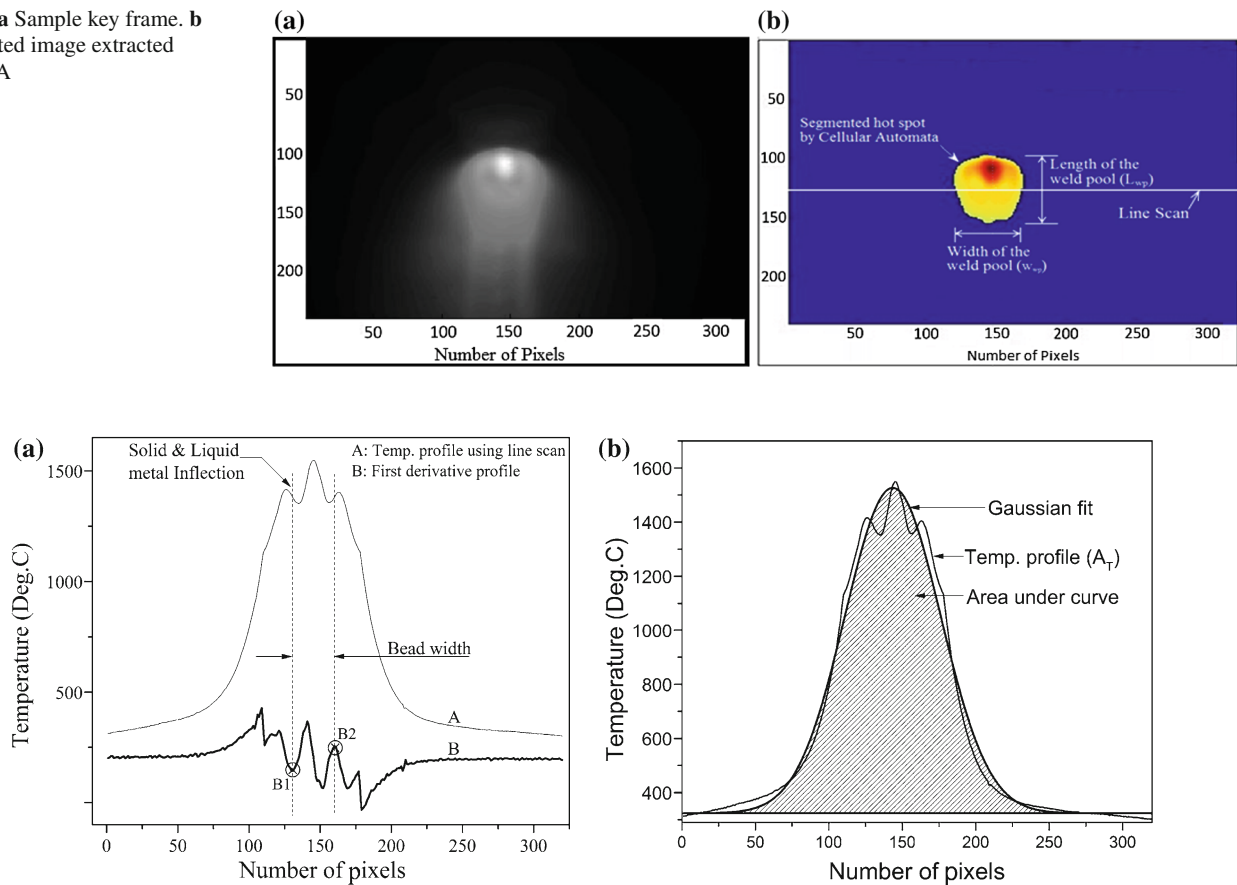


Fig. 5 Flow chart of CA algorithm

Feature extraction

Length  $L_{wp}(t)$  and width  $W_{wp}(t)$  of the weld pool, bead width computed from the first derivative curve of the Gaussian approximation temperature curve and thermal area ( $A_T$ ) under the Gaussian approximation of temperature profile are the image features extracted from the hot spot. The line scan is drawn on the segmented hot spot thermal images and adjusted until there is a better point of inflection in the thermal profile. The thermal intensity profile containing the temperature distributions throughout the line scan is extracted from the MATLAB software and analyzed in Origin software. The temperature distribution data profiles were processed in the Origin software for the feature identification. With advanced features of origin software, first derivative curve and Gaussian distribution curve were obtained. From the first derivative curve in Fig. 7a, the weld bead width was computed as the number of pixels between the inflection points B1 and B2 in the graph. Bead width computed as pixels was then converted to a linear dimension based on calibration using a measuring scale. It was found that one pixel correspond to 0.24 mm. To take into account the angle effect of IR camera on the bead width measurement, the computed weld bead width in linear dimension was multiplied by  $\cos 45$ . The computed weld bead width from the segmented IR image was compared with that of the actual measured bead width. There was good linear relationship between the computed and the actual bead width values with a minimum correlation coefficient of 0.8. Earlier work also reported similar accuracy values (Chen and Chin 1990; Banerjee et al. 1995; Menaka et al. 2005). So, CA algorithm accurately extract the molten weld pool image. It is found that the temperatures of the line of scan fits as a Gaussian like distribution and

**Fig. 6** **a** Sample key frame. **b** Segmented image extracted using CA



**Fig. 7** **a** First derivative curve of temperature profile. **b** Thermal area using Gaussian approximation

temperature profile is approximated by a Gaussian function. By plotting the Gaussian distribution curve with temperature as  $Y$ -axis and number of pixels as  $X$ -axis, the thermal area ( $A_T$ ) was obtained. The thermal area computed under a Gaussian fit approximated curve of the temperature profile is shown in Fig. 7b. The thermal area depends on the amount of heat input during welding and therefore the thermal area, length and width of the weld pool measured from the segmented image can be correlated with the measured depth of penetration. The extracted features were used as input variables for developing ANFIS and ANN based hybrid models. The Fig. 3 shows that the flow chart for the hybrid modeling.

### Data preparation

Ninety data sets were prepared using three lines of scans on each of the segmented image frame corresponding to thirty data points. These datasets were used to develop ANFIS and ANN models independently for predicting weld bead width (BW) and depth of penetration (DOP) during A-TIG welding of 6 mm thick 316LN austenitic stainless steel plates. The

extracted four image features along with current were correlated with the measured bead width and depth of penetration. The length  $L_{wp}(t)$  and width  $W_{wp}(t)$  of the hot spot region, distances between pixels of inflection point on the first derivative curve of Gaussian approximation temperature and welding current were correlated with physically measured weld bead width. Similarly, the length  $L_{wp}(t)$  and width  $W_{wp}(t)$  of the weld pool, and thermal area ( $A_T$ ) under the Gaussian approximation temperature profile and the welding current were correlated with the physically measured depth of penetration. Table 2 gives the input and output variables used for developing the weld bead width and the depth of penetration models.

### Development of ANFIS based models for estimating bead width and depth of penetration

The objective of ANFIS is to combine the best features of Fuzzy Systems and Neural Networks. The mechanism used in a FIS is mapping a given set of inputs to an output space using fuzzy logic. The FIS comprises (a) fuzzy sets and membership functions (b) fuzzy implication operator and

**Table 2** Input and output variables used for developing ANN and ANFIS models

Extracted image features considered for development of model (input variables)	Correlated with physically measured value (output variables)
1. Length of weld pool ( $L_{wp}$ )	Depth of penetration (DOP)
2. Width of weld pool ( $W_{wp}$ )	
3. Thermal area ( $A_T$ )	
4. Welding current	
1. Length of weld pool ( $L_{wp}$ )	Weld bead width (BW)
2. Width of weld pool ( $W_{wp}$ )	
3. Distance between B1 and B2 of first derivative curve ( $(B2 - B1) * 0.24 * \text{Cos}45$ )	
4. Welding Current	

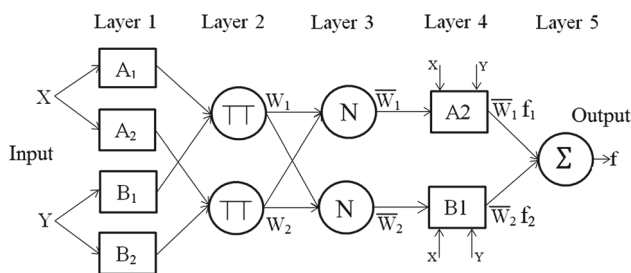


**Fig. 8** Five layer ANFIS architecture

(c) linguistic if-then rules. A membership function (MF) is a curve that defines mapping of each point in the input space to a membership value between 0 and 1 called the degree of membership. There are several types of membership functions viz. triangular, trapezoidal, Gaussian, generalized bell, sigmoidal, etc., of which triangular, Gaussian and generalized bell are considered in the present work, and their relative performance is compared. The typical ANFIS architecture is as shown in Fig. 8. The system architecture consists of five layers namely fuzzy layer, product layer, normalized layer, de-fuzzy layer and total output layer. The description of the computation involved in each layer is discussed in detail in our earlier paper (Nagesh and Datta 2010; Nagarajan et al. 1992).

Among the generated 90 data, 70 data were used for training, 10 data for checking and 10 data for testing the FIS. Two individual ANFIS models were developed each for predicting the weld bead width and depth of penetration. Takagi–Sugeno type FIS of zero order is used for model development. Three types of membership functions namely triangular (trimf), Generalized bell (gbell) and Gaussian (gaussmf) were selected and the degrees of membership is fixed as three representing the linguistic variables like low, medium and high. The membership function parameters are initially assigned by ANFIS. Then, FIS is generated implementing grid partitioning technique, which clusters all the data sets and creates the rules accordingly. Some of the basic rules extracted from the model for predicting the depth of penetration are as follows:

**Table 3** Parameters of the FIS developed

S. No.	Parameters	Numbers
1	Nodes	193
2	Nonlinear parameters	36
3	Training data pairs	70
4	Fuzzy rules	81
5	Linear parameters	81
6	Total parameters	117
7	Checking data pairs	20

- If (current is high) and ( $L_{wp}$  is low) and ( $W_{wp}$  is low) and (A is high), then (DOP is  $r_{25}$ )
- If (current is low) and ( $L_{wp}$  is high) and ( $W_{wp}$  is high) and (A is high) then (DOP is  $r_{55}$ )
- If (current is low) and ( $L_{wp}$  is low) and ( $W_{wp}$  is high) and (A is low) then (DOP is  $r_{74}$ )

where  $r_{25}$ ,  $r_{55}$ ,  $r_{74}$  are the linear/consequent parameters of the respective rules which is nothing but the output of the fuzzy rules. If-then rules are evaluated as given above and the output is expressed as linear equation. The entire operation is done in the ANFIS tool box. The parameters are shown in Table 3.

The back propagation and the least square technique were combined for training the FIS. Combination of back propagation and least square technique facilitate faster convergence and accurate results. The Error tolerance value chosen was 0.001. In order to select the optimized epoch number for the three types of membership functions used, the data set were trained with different epoch numbers and maximum epoch number below which over fitting of the model does not occur was chosen. The models were developed independently for predicting weld bead width and depth of penetration, the generalized bell and the triangular membership functions showed good membership function parametric tuning. For example, membership function parametric tuning observed before and

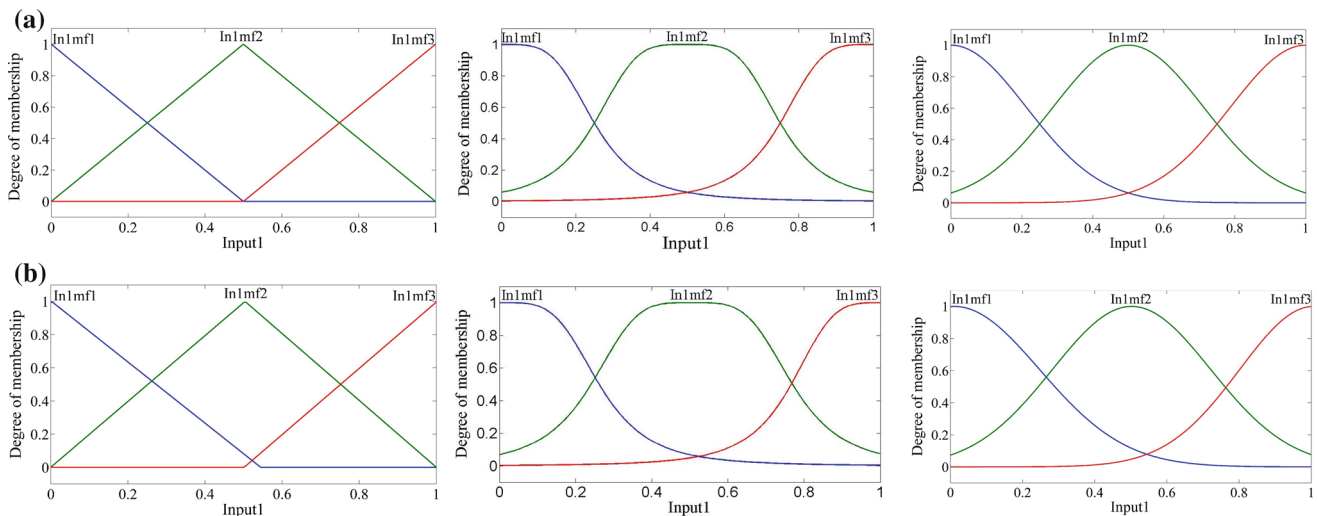


**Fig. 9** Parametric tuning of membership function for triangular, General-bell and Gaussian functions. **a** Before, **b** after for predicting the BW

**Table 4** Comparison of RMS error values for training and testing data of the bead width model

Membership function	RMS error value for prediction of bead width	
	Training	Testing
trimf	0.0102	0.0823
gbellmf	0.0149	0.023
gaussmf	0.0103	0.0516

after training of FIS for predicting weld bead width using the three membership functions is shown in Fig. 9a, b.

### Prediction of weld bead width

The comparison of RMS error values for training and testing data for predicting weld bead width using ANFIS models is given in Table 4.

From the above Table 4, it can be seen that the FIS using generalized bell (gbellmf) membership function produces the minimum RMS test error value of 0.023. It shows that bell membership function undergoes good membership function parametric tuning during the learning process. The RMS error using generalized bell MF is highest in training but least for testing because the generalization ability of the bell MF is better compared to the other two membership functions. The bell membership function is best for correlating the non-linear relation between the set of input and output variables for the dataset on bead width. Similarly for the dataset on depth of penetration, triangular membership function exhibits better generalization ability.

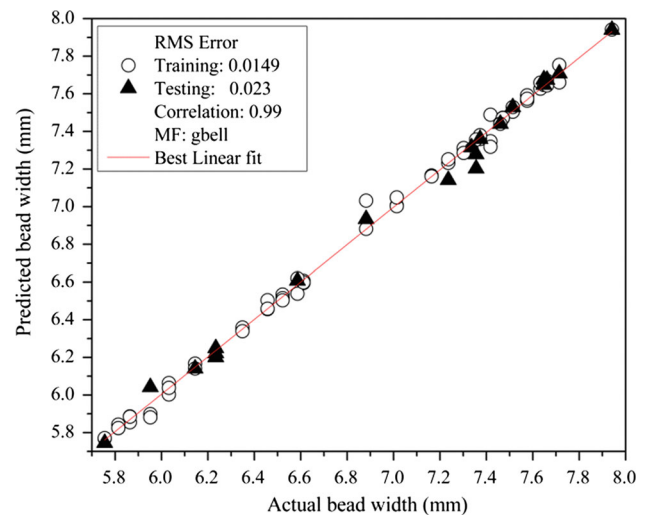


**Fig. 10** Plot between actual and predicted BW obtained using generalized bell function

The Fig. 10 clearly shows that there is a good correlation between the actual measured values and the predicted values of weld bead width. ANFIS model using bell membership function is saved into hard disk for further validation of the model.

### Prediction of depth of penetration

The comparison of the RMS error values obtained during training and testing data for the predicting depth of penetration using ANFIS models using different membership functions are given in Table 5. The ANFIS model with triangular membership function exhibited minimum RMS test error and hence saved to hard disk for validation of the model.



**Table 5** Comparisons between training and testing of RMS error values for DOP model

Membership function	RMS error value for prediction of depth of penetration	
	Training	Testing
trimf	0.0107	0.0341
gbellmf	0.0044	0.0404
gaussmf	0.0038	0.0390

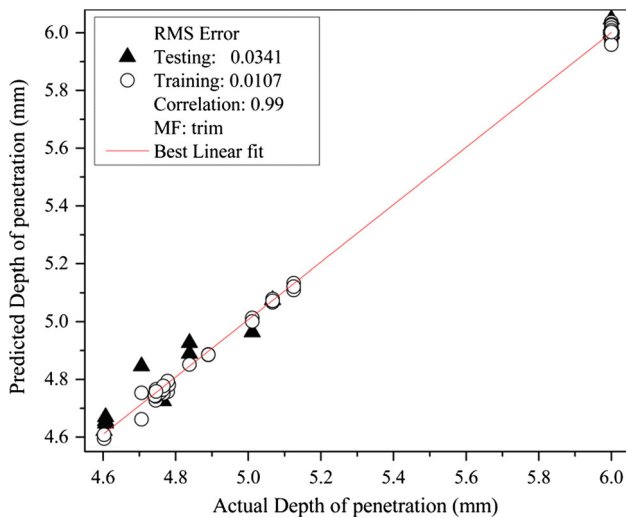


**Fig. 11** Plot between actual versus predicted DOP obtained using trimf

The Fig. 11 clearly shows that there was good agreement between the actual values and the predicted values of depth of penetration.

**Artificial neural network model development for estimating bead width and depth of penetration**

The datasets prepared with 90 data consists of extracted features from IR thermal images and current as input variables and physically measured bead width and depth of penetration as output variables for development of two independent models. The dataset was fully randomized before the generation of the model. Among the available 90 data, 70 data were used for training and 20 were used for testing the neural network models. The randomized 90 data points were normalized between 0 and 1 by the transformation formula given below.

$$X_N = (X - X_{min}) / (X_{max} - X_{min}); \text{ Data normalization}$$

The new Feed Forward back propagation neural network was created with one hidden and one output layer using a MATLAB neural network tool box. The entire neural network features used for the model development are as shown Fig. 12.

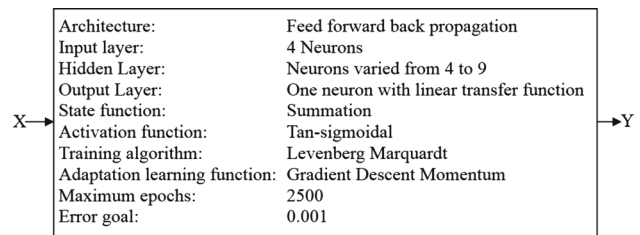


**Fig. 12** Neural network architecture parameters

**Table 6** Performances of the proposed neural networks for bead width model

Network architecture	Root mean square error	
	Training	Testing
4-4-1	0.0585	0.06
4-5-1	0.0906	0.0968
4-6-1	0.0322	0.0389
4-7-1	0.0958	0.1018
4-8-1	0.0533	0.0991
4-9-1	0.0638	0.0771

**Artificial neural network model on bead width**

The four input variables consist of current, length and width of the weld pool and the bead width estimated from the first derivative curve. The output consists of measured weld bead width. The network was trained with various hidden neurons. The performance of the neural network models with various numbers of hidden neurons in terms of training and testing based RMS error values is compared Table 6. The neural network model with six hidden neurons was found to exhibit minimum RMS test error. Therefore, the neural network model with 4-6-1 network architecture was chosen with all its weights and biases for further validation. The finalized neural network input, output layer weights and biases are given in Tables 7 and 8.

The Fig. 13 shows that the comparison between predicted and measured bead width of both the training and the test data. There was excellent agreement between the predicted and measured values.

**Artificial neural network model on depth of penetration**

The input variables consists of current, length and width of the weld pool and the thermal area under the Gaussian approximation of the temperature profile and the output variable consist of measured depth of penetration. The neural network models were developed with varying number of hidden neurons and their performance were compared in terms of the training and testing RMS error values as given in Table 9.

**Table 7** Weight values from input layer to hidden layer Lw(1,1) for bead width

Node number	Input parameters (input weights(1,1))						
	Current	Length of weld pool	Width of weld pool	Distance pixels from first derivative curve			
1	-0.21533	-1.6577	-2.57	-1.3028			
2	-0.31753	-0.06218	-3.2824	-0.27353			
3	-4.8595	4.1587	-0.18945	-0.23357			
4	1.1397	0.66855	-6.6301	-0.29776			
5	-1.068	-0.20999	-1.7039	-0.12676			
6	-1.3525	2.7325	-1.4262	-2.0808			
Layer weight	Lw(2,1)					Lw(3,2)	
Node number	1	2	3	4	5	6	
Weight values	-0.13169	-2.1846	-0.19761	0.39153	2.2786	0.18486	-2.168

**Table 8** Weight and bias values from hidden layer to output layer for bead width

Bias	Layer 1						Layer 2	Layer 3
	1	2	3	4	5	6		
Weight values	2.356	-1.1578	-1.3909	-1.4755	-0.97746	-1.4228	-0.0065751	-0.41228

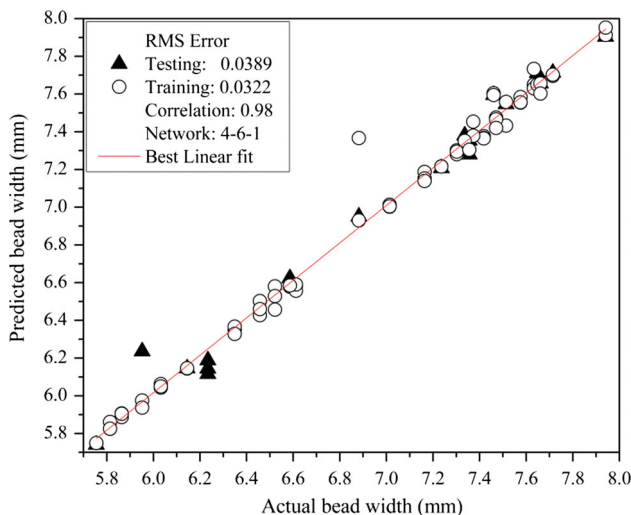


**Fig. 13** Plot between predicted and measured bead width

Among all the trained network architecture, the network with six hidden neurons was found to produce RMS test error value of 0.0138. Therefore, the model with 4-6-1 network architecture was chosen for predicting depth of penetration. The finalized neural network input and output layer weight and bias of optimized network architecture of 4-6-1 are given in Tables 10 and 11. The comparison of the predicted and measured values is shown in Fig. 14. There was excellent agreement between the measured and predicted values of depth of penetration.

**Table 9** Performances of neural networks for predicting depth of penetration

Network architecture	Root mean square error	
	Training	Testing
4-4-1	0.0548	0.0885
4-5-1	0.0278	0.0648
4-6-1	0.0306	0.0138
4-7-1	0.0053	0.0198
4-8-1	0.0369	0.0685
4-9-1	0.0579	0.0825

**Validation of the ANFIS and ANN models**

To check the performance of the developed ANFIS and ANN models, validation experiments were conducted. The performance of both the ANFIS and ANN models in predicting the weld bead width is presented below (Fig. 15).

**Validation for weld bead width models**

The Table 12 shows the comparison between physically measured bead width values and the predicted bead width values of ANFIS and ANN models. Figures 16 and 17 compare the measured values with models predicted values. There was good agreement between the measured and predicted bead width values. The RMS error for predicting weld bead width

**Table 10** Weight values from input layer to hidden layer for depth of penetration

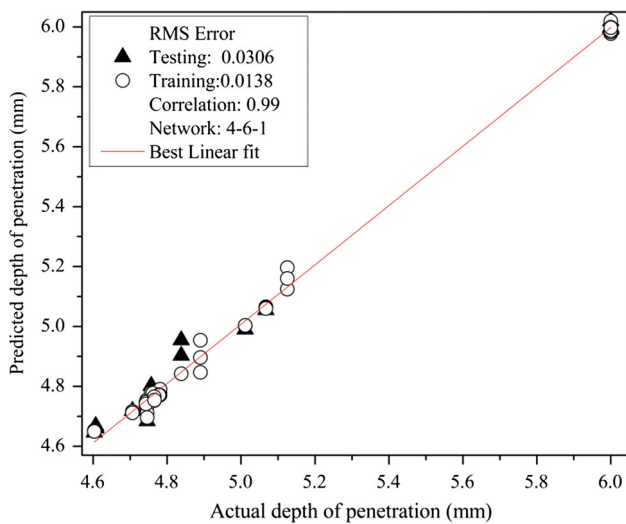
Node number	Input parameters			
	Current	Length of weld pool	Width of weld pool	Thermal area ( $A_T$ )
1	4.4724	-1.1924	-3.8163	-1.8271
2	4.7423	0.66791	-3.4037	-0.47294
3	2.4592	-0.25055	-0.53008	2.4284
4	5.7327	1.0364	-0.31831	2.3887
5	-1.5838	2.0203	0.36914	1.4981
6	4.7475	-4.2643	-2.488	-1.8516

Layer	Lw(2,1)						Lw(3,2)
Node number	1	2	3	4	5	6	
Weight values	-1.5952	1.3118	-1.0315	1.2216	0.17953	2.5338	0.65134

**Table 11** Weight and bias values from hidden layer to output layer for depth of penetration

Bias	Layer 1						Layer 2	Layer 3
	1	2	3	4	5	6		
Weight values	2.1892	0.35834	0.25403	-1.9211	-3.8359	3.6675	-0.025578	-0.45764



**Fig. 14** Plot between predicted and measured depth of penetration

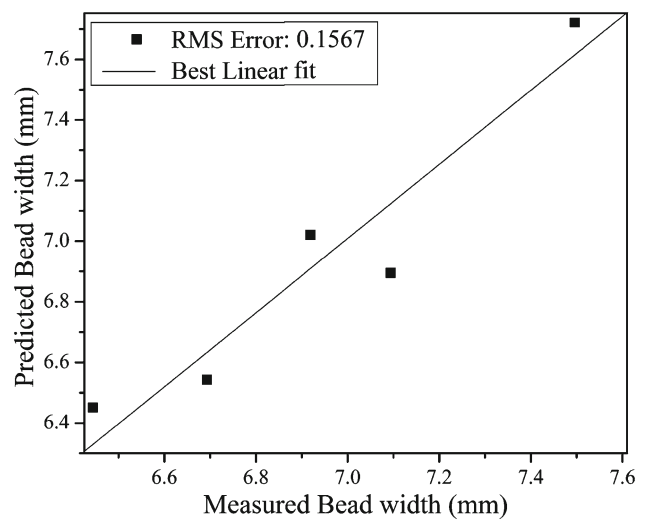


**Fig. 15** Plot between physically measured and predicted bead width using ANN

using the ANFIS model was 0.11 while for the ANN model was 0.15 for the validation data set.

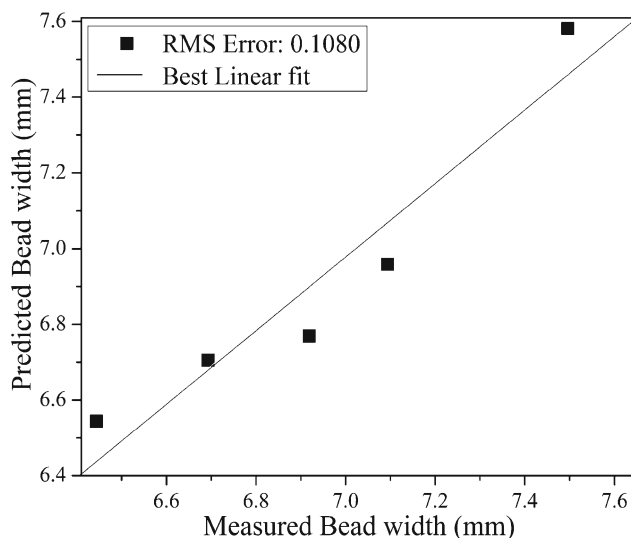
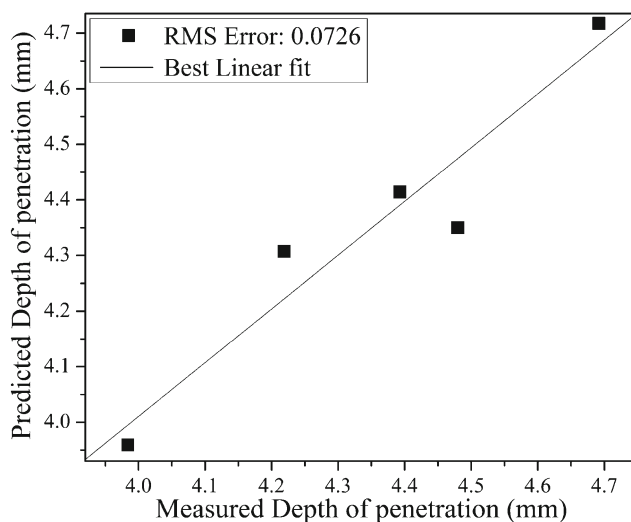
Validation for depth of penetration models

Table 13 shows the comparison between the physically measured depth of penetration with the ANFIS and ANN predicted depth of penetration values for the validation data set. Figures 17 and 18 compare the predicted and measured values of depth of penetration for the ANFIS and ANN models.

There was good agreement between the predicted and measured values of depth of penetration. The RMS error for predicting the depth of penetration using ANFIS model was 0.07 while for ANN model, it was 0.21 for validation data. Both the ANFIS and ANN models were found to estimate the weld bead width and the depth of the penetration accurately for the validation data set. The RMS error values were lower for ANFIS based models. Also, Generation and execution of ANFIS based models were taking less time and

**Table 12** Comparison between the physically measured bead values and the models predicted values

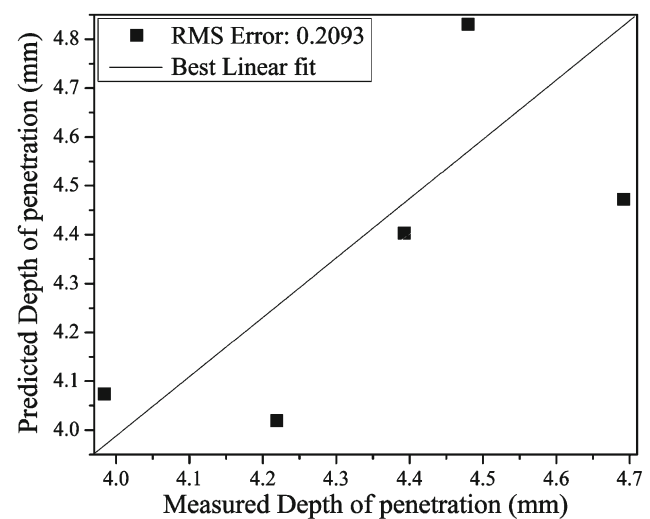
Physically measured weld bead width in mm	Predicted weld bead width in mm	
	ANN	ANFIS
6.444	6.451	6.544
6.693	6.543	6.7052
6.919	7.019	6.769
7.094	6.894	6.958
7.496	7.72	7.581

**Fig. 16** Plot between physically measured and ANFIS predicted BW**Fig. 17** Plot between physically measured and ANN predicted DOP

therefore may be beneficial while applying for real time welding process monitoring and control.

**Table 13** Comparison between the measured and models predicted depth of penetration

Physically measured depth of penetration in mm	Predicted depth of penetration in mm	
	ANN	ANFIS
3.984	4.074	3.959
4.219	4.019	4.307
4.393	4.403	4.414
4.480	4.830	4.350
4.692	4.472	4.717

**Fig. 18** Plot between physically measured and ANFIS predicted DOP

## Conclusions

1. Cellular automata image processing has been successfully applied for the first time to identify the hot spot in the IR thermal image of the weld pool. The algorithm has been found to be efficient in identifying the hot spot in the IR thermal image. Therefore, a methodology using CA has been developed for extracting the hot spot region from IR thermal images of the weld pool.
2. The ANFIS based models have been developed for estimating the weld bead width and depth of penetration from the extracted image features and the current values used for making the weld joint. RMS error of validation data set for predicting bead width is 0.11 and for predicting depth of penetration is 0.07.
3. The ANN model with a network architecture of 4-6-1 was chosen for predicting weld bead width and depth of penetration as it exhibited a minimum RMS error on the test data set. RMS error of validation data for predicting the weld bead width was 0.15 and for predicting depth of penetration was 0.209 by ANN models.

4. The intelligent model combining image processing with ANFIS was found to predict weld bead width and depth of penetration more accurately from the IR thermal image of the weld pool. The performances of the ANFIS models in terms of the RMS error on the validation data set were better compared to ANN models. Also the model involving ANFIS was found to take lesser computation time and would be suitable for real time applications.

## References

- A, Sun, & E, Kannatey-Asibu, Jr. (1999). Sensors systems for real-time monitoring of laser weld quality. *Journal of Laser Applications*, 11(4), 153–168.
- Banerjee, P., Govardhan, S., Wickle, H. C., Liu, J. Y., & Chin, B. A. (1995). Infrared sensing for on-line weld geometry monitoring and control. *Journal of Engineering for Industry*, 117(8), 323–330.
- Chen, W., & Chin, B. A. (1990). Monitoring joint penetration using infrared sensing techniques. *Welding Research Supplement*, 69(4), 181s–185s.
- Edwin Raja Dhas, J., & Kumanan, S. (2007). ANFIS for prediction of weld bead width in submerged arc welding process. *Journal of Scientific and Industrial Research*, 66(4), 335–338.
- Farson, D., Richardson, R., & Li, X. (1998). Infrared measurement of base metal temperature in gas tungsten arc welding. *Welding Journal*, 77(9), 396–401.
- Ghanty, P., Paul, S., Mukherjee, D. P., Vasudevan, M., Pal, N. R., & Bhaduri, A. K. (2007). Modeling weld bead geometry using neural network for GTAW of an austenitic stainless steel. *Science and Technology of Welding and Joining*, 12(7), 649–658.
- Ghanty, P., Vasudevan, M., Chandrasekhar, N., Mukherjee, D. P., Maduraimuthu, V., Pal, N. R., et al. (2008). Artificial neural network approach for estimating weld bead width and depth of penetration from infrared thermal image of weld pool. *Science and Technology of Welding & Joining*, 13(4), 395–401.
- Graham, G. M. & Ume, I. C., (1997). Automated system for laser ultrasonic sensing of weld penetration. In it AIM proceedings of the 1997 1st IEEE/ASME international conference on advanced intelligent mechantronics, Tokyo, Japan, June, 16–20, 59.
- Gowtham, K. N., Vasudevan, M., Maduraimuthu, V., & Jayakumar, T. (2011). Intelligent modeling combining adaptive neuro fuzzy inference system and genetic algorithm for optimizing welding process parameters. *Metallurgical and Materials Transactions B*, 42(2), 385–392.
- Hamamci, A., Unal, G., Kucuk, N., & Engin, K. (2010). Cellular automata segmentation of brain tumors on post contrast MR images. In *Proceedings of the 13th international conference on medical image computing and computer-assisted intervention*. Part III, pp. 137–146.
- Huang, R. S., Liu, L. M., & Song, G. (2007). Infrared temperature measurement and interference analysis of magnesium alloy in hybrid laser-GTA welding process. *Materials Science and Engineering A*, 447, 239–243.
- Huang, W., & Kovacevic, R. (2009). Feasibility study of using acoustic signals for online monitoring of the depth of weld in the laser welding of high strength steels. *Part B: Journal of Engineering Manufacture*, 223, 343–361.
- Huang, Wei, & Kovacevic, Radovan. (2011). A laser based vision system for weld quality inspection. *Sensors*, 11(1), 506–511.
- Hyunsung Park and Seun Rhee. (1999). Estimation of weld bead size in CO<sub>2</sub> laser welding by using multiple regression and neural network. *Journal of Laser Applications*, 11(3), 143–150.
- Isa, N. A. M., Salamah, S. A., & Ngah, U. K. (2009). Adaptive fuzzy moving K-means clustering algorithm for image segmentation. *IEEE Transactions on Consumer Electronics*, 55(4), 2145–2153.
- Kovacevic, R., Zhang, Y. M., & Ruan, S. (1995). Sensing and control of weld pool geometry for automate GTA welding. *ASME Journal of Engineering for Industry*, 117(2), 210–222.
- Kovacevic, R., & Zhang, Y. M. (1997). Real time image processing for monitoring of free weld pool surface. *ASME Journal of Manufacturing Science and Engineering*, 19(2), 119–169.
- KAZAR, O., & SLATNIA, S. (2011). Evolutionary cellular automata for image segmentation and noise filtering using genetic algorithms. *Journal of Applied Computer Science and Mathematics*, 5(10), 33–40.
- Kumar, T., & Sahoo, G. (2010). A Novel method of edge detection using cellular automata. *International Journal of Computer Applications*, 9(4), 0975–8887.
- Menaka, M., Vasudevan, M., Venkatraman, B., & Raj, B. (2005). Estimating bead width and depth of penetration during welding by infrared thermal, imaging. *Journal of British Institute of NDT*, 47(4), 564–568.
- Nagesh, D. S., & Datta, G. L. (2010). Genetic algorithm for optimization of welding variables for height to width ratio and application of ANN for prediction of bead geometry for TIG welding process. *Applied Soft Computing*, 10(3), 897–907.
- Nagarajan, S., Banerjee, P., Chen, W. H., & Chin, B. A. (1992). Control of welding process using infrared sensors. *IEEE Transactions on Robotics and Automation*, 8(1), 86–93.
- Subashini, L., & Vasudevan, M. (2012). Adaptive neuro-fuzzy inference system (ANFIS) based model for predicting the weld bead width and depth of penetration from the infra-red thermal image of the weld pool. *Metallurgical and Materials Transactions B*, 43(1), 145–154.
- Chokkalingham, S., Chandrasekhar, N., & Vasudevan, M. (2012). Predicting depth of penetration and weld bead width from infra-red thermal image of weld pool using artificial neural network. *Journal of Intelligent Manufacturing*, 23(5), 1995–2001.
- Vasudevan, M., Chandrasekhar, N., Maduraimuthu, V., Bhaduri, A. K., & Raj, B. (2010). Real-time monitoring of weld pool during GTAW using infra-red thermography and analysis of infra-red thermal images. *Welding in the World*, 55(7), 83–89.
- Vasudevan, M., (2007). Computational and experimental studies on arc welded austenitic stainlesssteels, PhD Thesis, Indian Institute of Technology, Chennai.
- Wolfram, S. (1986). Theory and applications of cellular automata. World Scientific, ISBN: 9971–50-123-6.
- Zhang, Y. M. (2008). *Real time weld process monitoring*. Cambridge, England: Wood Head Publishing and Maney Publishing.